

Cite this: DOI: 10.1039/c8dt01120f

The unsuspected influence of the pyridyl-triazole ligand isomerism upon the electronic properties of tricarbonyl rhenium complexes: an experimental and theoretical insight†

Jinhui Wang,^{‡a} Béatrice Delavaux-Nicot,^{id b,c} Mariusz Wolff,^{id §d}
Sonia Mallet-Ladeira,^e Rémi Métivier,^{id f} Eric Benoist^a and
Suzanne Fery-Forgues^{id *a}

Two isomeric tricarbonyl rhenium(i) complexes, **ReL1** and **ReL2**, that possess a 2-pyridyl-1,2,*n*-triazole (pyta) ligand (*n* = 4 and 3, respectively) connected to a 2-phenylbenzoxazole (PBO) moiety, were synthesized in good yields. The X-ray structures showed that in **ReL1** the PBO moiety and the pyta ligand almost form a right angle hindering electron delocalization, while in **ReL2** their nearly planar arrangement favors the electron delocalization in the whole organic ligand. Therefore, the nature of the ligand significantly influences the electron distribution in the two complexes, as indicated by the results of TD-DFT calculations. An electrochemical study highlighted that, by comparison with **ReL2**, the smaller HOMO–LUMO energy gap of **ReL1** is in line with its lower first reduction potential. From a spectroscopic viewpoint, both complexes emitted phosphorescence in organic solvents, with distinct color and intensity. They also emitted in the solid state, but only **ReL1** showed significant aggregation-induced phosphorescence emission (AIPE). This complete study sheds light on the crucial role of structural isomerism of the triazole group, which has been unsuspected for a long time although it can govern the geometry and electronic properties of rhenium complexes. It is shown for the first time that grafting a non-coordinated π -conjugated fragment on the N(4) atom of a 1,2,4-triazole group can be of high value for the design of efficient light-emitting materials based on rhenium complexes.

Received 23rd March 2018,

Accepted 29th May 2018

DOI: 10.1039/c8dt01120f

rsc.li/dalton

^aSPCMIB, CNRS UMR5068, Université Toulouse III Paul-Sabatier, 118 route de Narbonne, 31062 Toulouse cedex 9, France. E-mail: sff@chimie.ups-tlse.fr

^bLaboratoire de Chimie de Coordination, CNRS UPR 8241, 205 route de Narbonne, 31077 Toulouse Cedex 4, France

^cUniversité de Toulouse UPS, INPT 31077 Toulouse Cedex 4, France

^dInstitute of Chemistry, Department of Crystallography, University of Silesia, 9th Szkolna St., 40-006 Katowice, Poland

^eService commun RX, Institut de Chimie de Toulouse, ICT- FR2599, Université Toulouse III Paul-Sabatier, 118 route de Narbonne, 31062 Toulouse cedex 9, France

^fPPSM, ENS Cachan, CNRS, Université Paris-Saclay, 94235 Cachan, France

†Electronic supplementary information (ESI) available: Experimental details, including proton numbering for NMR; picture of crystals, molecular views, and CIF data; additional computational, electrochemical and spectroscopic data. CCDC 155800 and 1555801. For ESI and crystallographic data in CIF or other electronic format see DOI: 10.1039/c8dt01120f

‡Institute of Drug Discovery Technology, Ningbo University, Ningbo 315211, China.

§Institut für Anorganische Chemie, Johannes Kepler Universität Linz, Altenberger Straße 69, 4040 Linz, Austria.

Introduction

Since the discovery of their photoluminescence properties in 1974,¹ the air and water stable tricarbonyl rhenium(i) complexes have been widely studied from a photophysical viewpoint² and have proven to be valuable photoluminescent cellular imaging agents.^{3–6} In addition to allowing detection in the visible, they strongly absorb in the middle infrared where light penetration in tissues is optimal, and thus they enable bimodal IR and luminescence bioimaging.^{7,8} Some of them could also serve as new agents for the delivery of carbon monoxide to biological targets under the control of light, in the frame of phototherapy.⁹ These complexes are very versatile because they also possess three facial positions available for substitution by various organic or inorganic ligands, which allow a wide control over their physical, spectroscopic and biological properties.^{5,6} In this context, pyridyl-triazole (pyta) ligands are of special interest. They combine the coordination abilities of pyridine and triazole rings, have strong σ -electron-donating capability, and can be functionalized much more

easily than the ubiquitous bipyridine-based ligands. Moreover, the triazole ring has various isomeric forms, the 1,2,3-isomer being by far the most popular since the rediscovery of Huisgen “click” reaction by the Sharpless group.¹⁰ Each isomer offers distinct substitution patterns and coordination abilities potentially useful to modulate the complex properties.¹¹ Recently, Lo *et al.*¹² and Bertrand *et al.*¹³ have compared isomeric tricarbonyl Re(I) complexes in which a 2-pyridyl group and an aromatic group are respectively borne by the C(4) and N(1) atom of the 1,2,3-triazole fragment, and *vice versa*. Both teams have shown interesting differences in the optical transitions of the corresponding complexes. To our knowledge, other triazole isomers have not been considered.

The aim of the present work was to compare the behavior of two substituted tricarbonyl Re(I) complexes that differ by the position of the third nitrogen atoms in their triazole ring. Specifically, the **ReL1** complex contains the 3-(2-pyridyl)-1,2,4-triazole fragment, some derivatives of which have been recently used for the preparation of luminescent iridium complexes.¹⁴ The **ReL2** complex includes the well-known 4-(2-pyridyl)-1,2,3-triazole fragment. In order to improve the emission properties, the idea was to combine the pyta ligand with an organic dye moiety. To this aim, a 2-phenylbenzoxazole (PBO) moiety was chosen for its excellent stability and fluorescence efficiency, both in solution and in the solid state.¹⁵ An originality of this design is that a large π -electron conjugated moiety not directly involved in Re complexation is linked to a triazole nitrogen atom, on the pyta fragment. To the best of our knowledge, this design is surprisingly unprecedented for complexes that incorporate a pyta fragment, whose nitrogen atoms usually do not bear more than a phenyl group as an aromatic substituent.

The synthesis and crystallographic characterization of complexes **ReL1** and **ReL2** were reported, along with the electrochemical, spectroscopic and photophysical studies. Experimental data were supported by TD-DFT calculations. At first sight, both complexes look very similar, but they behave in a very different way. This study reveals how the nature of the pyta isomer and the functionalization of this ligand by a PBO moiety can be of prior importance, especially regarding the impact on the photoluminescence properties. Thus, it paves the way towards new families of strongly emissive rhenium complexes substituted by various organic fluorophores.

Results and discussion

Synthesis

The synthetic pathways for the preparation of the tricarbonyl rhenium complexes are shown in Fig. 1. First of all, 6-nitro-2-phenylbenzoxazole (**1**) was obtained in good yield by classical condensation of 2-amino-5-nitrophenol with benzoic acid in the presence of polyphosphoric acid, and then it was catalytically reduced to afford the corresponding amino derivative (**2**). From this compound, ligand **L1** was obtained in modest yield

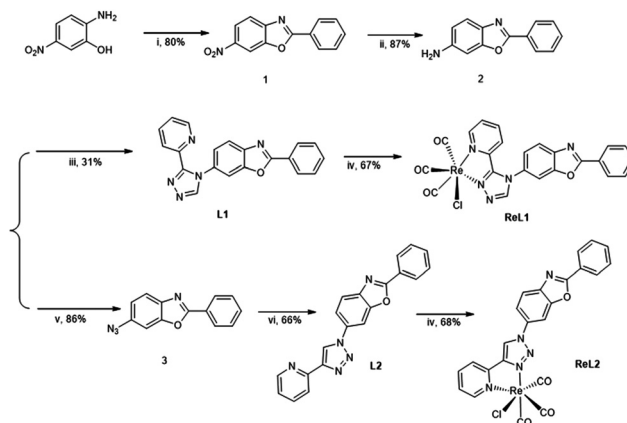


Fig. 1 Conditions: (i) Benzoic acid, polyphosphoric acid, 110 °C, 16 h; (ii) 10% Pd/C, H₂, MeOH/CHCl₃, 6 bars, r.t., 24 h; (iii) dimethoxy-*N,N*-dimethylmethanamine, pyridine-2-carbohydrazide, acetic acid, CH₃CN, 50–120 °C, 16 h; (iv) [Re(CO)₅Cl], MeOH, 65 °C, 16 h. (v) HCl (6 N), NaNO₂, NaN₃, 0 °C to r.t.; (vi) 2-ethynylpyridine, Cu(OAc)₂·H₂O, NaAsc., CH₃CN, r.t., 16 h.

through a one-pot condensation reaction as described in the literature.¹⁶ Unfortunately, up to now, all attempts to improve the formation of the pyridyl-1,2,4-triazole scaffold failed. The preparation of ligand **L2** went through an azide derivative (**3**) that was subsequently condensed with 2-ethynylpyridine *via* a Copper(I) catalyzed alkyne–azide cycloaddition using classical click reaction conditions. Although **L2** required an additional step of synthesis, its overall yield was better than **L1** (40% *vs.* 22%). As expected, the formation of the pyridyl-1,2,3-triazole scaffold was thus easier than that of the other isomer. The corresponding tricarbonyl rhenium(I) complexes **ReL1** and **ReL2** were then easily prepared in good yields (*ca.* 66%) by reacting the commercial precursor [Re(CO)₅Cl] with **L1** or **L2** in refluxing methanol. All compounds were obtained with good overall yields after purification by chromatography. Ligands and complexes were unambiguously identified by ¹H and ¹³C NMR, elemental microanalysis and high resolution mass spectrometry. Detailed synthetic procedures and characterization data are given in the Experimental section. It is noteworthy that in infrared spectroscopy, the characteristic $\nu(\text{CO})$ stretching bands of the complexes appeared at 2025, 1919, 1884 cm⁻¹ for **ReL1**, and at 2030, 1920 and 1903 cm⁻¹ for **ReL2**, with average values at 1942 and 1951 cm⁻¹, respectively. According to a recent work from Sarkar’s group, the position of these bands can be correlated with the electron density on the metal center, and hence with the overall donor ability of the ligand.¹⁷ In our case, ligand **L1** would be a slightly better electron donor than **L2**, very close to a bipyridyl ligand (ν_{average} of Re(bpy)(CO)₃Cl: 1943 cm⁻¹).¹⁸

Crystal structures

Fortunately, single crystals of complexes **ReL1** and **ReL2** suitable for X-ray crystallography analysis were successfully grown

by slow evaporation of organic solvents. Full crystallographic data, as well as data regarding hydrogen bonding and packing mode, are reported as ESI,[†] along with the geometric parameters of complexes such as bond lengths and bond angles (Tables S1–S4, Fig. S1 and S2[†]).

As illustrated in Fig. 2, both complexes showed many similarities. Regarding the rhenium environment, they present a distorted octahedral geometry. As expected, the Re(i) atom is coordinated to three carbonyl ligands arranged in a *facial* configuration, one chlorine atom, and two nitrogen atoms of the pyta moiety. Two carbonyl groups C(2)–O(2) and C(3)–O(3) along with pyridine nitrogen atom N(2) and triazole nitrogen atom N(3) occupy the equatorial positions. The third carbonyl group and one chlorine atom occupy the axial positions and coordinate to the Re(i) atom linearly with an angle equal to 177.0(2)° in **ReL2**, and to 176.1(2)°/174.8(2)° in **ReL1** for conformational type I and II, respectively (*vide infra*). Examining now the pyta moiety, for both complexes, only a small twist angle of approximately 5° was observed between the triazolyl and pyridyl components. All bond length and angle values are in line with those reported for other rhenium complexes, either containing various azole ligands combined with a 2-pyridyl group,^{19–21} or based on 4-(2-pyridyl)-1,2,3-triazole ligands and developed by our team.²²

However, significant differences were also revealed by the crystallographic study. Complex **ReL1** crystallized in the monoclinic $P2_1/n$ space group with two crystallographically distinct molecules of complex and one acetonitrile molecule in the asymmetric unit. Most importantly, in one of the molecules,

the free rotation between the triazole group and the PBO moiety allowed the latter to occupy two distinct positions. In 68% of the cases (type I), the oxygen atom of the benzoxazole group and the chlorine atom of the coordination sphere pointed opposite directions, and the benzoxazole group was twisted by 16.2(6)° with respect to the phenyl group. In the remaining 32% (type II), the benzoxazole oxygen and the chlorine atom pointed in the same direction, and the benzoxazole group was twisted by 21.7(1)° with respect to the phenyl group. The angle between the benzoxazole group and the triazole group was 64.0(2)° for the first molecule, and 69.3(3)°/82.0(6)° for the second one (type I and type II, respectively). Complex **ReL2** crystallized in the monoclinic $P2_1/c$ space group with one acetone molecule per molecule of complex. No disorder was observed. The main feature is that the whole organic ligand was almost planar, the angle between the benzoxazole group and the triazole group being only 9.0(2)°.

Therefore, substitution of the triazole fragment by the pyridyl and PBO groups in adjacent positions in **ReL1** induces strong steric hindrance, which does not exist with the 1,3-substitution pattern of **ReL2**. The conjugated systems of the complexes are strongly impacted. The marked bending of the organic ligand in **ReL1** suggests that the π -electron systems of the pyta and PBO moieties have little interaction and should behave almost independently, while the planarity of these moieties in **ReL2** should promote strong interaction between them. To the best of our knowledge, this is the first time that such a difference appears for two rhenium complexes only differing by the isomerism of their pyta ligand.

Regarding now the molecular packing (Table S2, Fig. S1 and S2[†]), for **ReL1** (type I), π -stacking interactions occur between two parallel triazole rings with a centroid-to-centroid distance of 3.6 Å. However, molecules were slipped laterally, and no significant overlap of the PBO aromatic systems was observed. The molecular arrangement was compact and well structured by a network of intermolecular hydrogen bonding interactions. For type II molecules, the network seemed to be looser than in the former case. In contrast, **ReL2** complexes exhibited crossed arrangement, which is quite frequent for PBO derivatives.¹⁵ Stacked molecules were roughly situated in parallel planes, offset from one another and oriented in the same direction. They exhibited partial overlap of their aromatic systems. Slipped π - π stacking interactions take place between the 2-phenyl ring of one molecule and the benzene ring of its closest neighbor with a centroid-to-centroid distance of 3.7 Å, and between the oxazole ring of one molecule and the triazole ring of the other one, with a centroid-to-centroid distance of 3.6 Å. Therefore, π -stacking interactions in the solid state were stronger in **ReL2** than in **ReL1**.

TD-DFT calculations

Computational studies based on the time dependent density functional theory (TD-DFT) method at the PBE1PBE/LANL2DZ/6-31+G** level were performed considering the two complexes in dichloromethane (DCM). At the S_0 ground state level, calculations gave a very good estimation of a number of coordinat-

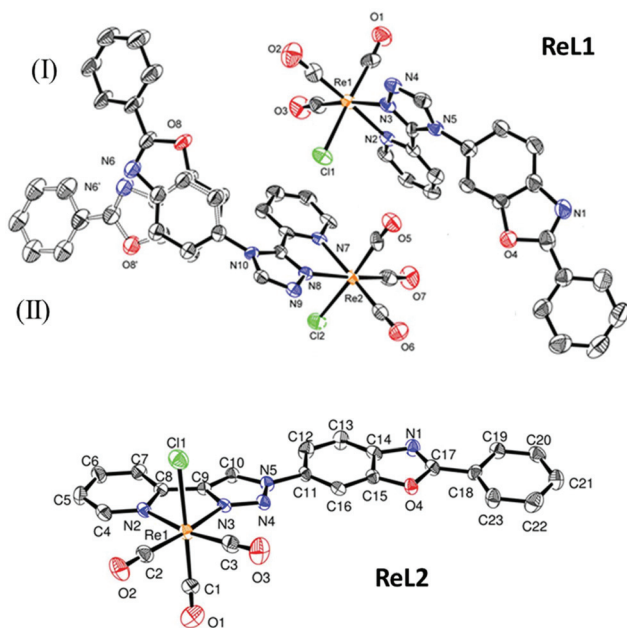


Fig. 2 Top: Molecular view of the asymmetric units of complex **ReL1**. The molecule on the left side may have two conformations (types I and II). Bottom: Molecular view of complex **ReL2**. Thermal ellipsoids are drawn at the 50% probability level. Solvent molecules and H atoms are omitted for clarity.

ing bond lengths and angle values, which differed at the most by 0.05 Å and 3°, respectively, with respect to the corresponding X-ray crystallographic data (Tables S3 and S4†). Upon excitation, the geometries of the first singlet excited state S_1 and first triplet excited state T_1 kept octahedral conformation. However, in comparison with the ground-state, the Re–N bonds in S_1 state were shortened by about 0.05–0.06 Å, while Re–CO bonds were elongated by *ca.* 0.04–0.06 Å, which indicates that the CO ligands tend to break away from the Re atom and that the chelate ligand is getting close to the Re atom in the excited state. This effect can be attributed to the electron density transfer from the Re–CO bonding orbital to the π^* orbital of the organic ligand upon excitation. The same trend was observed for the lowest triplet state T_1 of both complexes. Other data are given in the ESI (Tables S5–S8†). An interesting point to note is that the electrostatic potentials appeared to be more localized in definite areas in **ReL1** than in **ReL2** (Fig. S3†).

The composition and energy levels of frontier molecular orbitals (FMOs) are presented in Fig. 3 and Table S9.† As expected for both complexes, the two highest occupied orbitals (HOMO and HOMO–1) are almost totally centered on the rhenium moiety. In contrast, the HOMO–2 is dominantly localized on the organic ligand, and more precisely on the PBO moiety with a contribution around 75% for **ReL2**, and up to

96% for **ReL1**. On the other hand, the first three lowest unoccupied orbitals (LUMOs) are predominantly based on the organic moiety with π^* character, with the difference that orbitals of **ReL2** extend significantly over the whole organic ligand, while those of **ReL1** are well centered either on the pyta moiety (LUMO and LUMO+2) or on the PBO moiety (LUMO+1). Therefore, the nature of the triazole group and its functionalization by a PBO moiety on a different position influence the electron distribution over the complexes. It also has a strong effect on the energy levels. The most striking feature is the decrease of the LUMO energy in **ReL1** with respect to **ReL2**, while the respective energy levels of the LUMO+1, HOMO and HOMO–1 orbitals are almost unchanged in both compounds (Fig. 4). In contrast, it is interesting to see that isomerism has a weak effect on the composition of orbitals involved in the T_1 state, which are centered on the metal environment and on the pyta moiety, with no contribution of the PBO moiety for both complexes (Fig. 5). The calculated absorption and emission energies (Tables S10–S13†) will be discussed below in comparison with the experimental data.

Electrochemical study

The electrochemical behavior of the complexes was studied by cyclic voltammetry (CV) and Osteryoung square wave voltammetry (OSWV) measurements in DCM at room temperature. In the OSWV anodic part, complexes **ReL1** and **ReL2** are characterized by two oxidation processes around 1.46 and 1.76 V (Table 1 and Fig. 6a). The former process can be assigned to an irreversible $\text{Re}(i)$ oxidation process^{21,23} which is slightly easier for complex **ReL1** than for **ReL2**. It could be expected that in comparison with the folded structure of the organic moiety in compound **ReL1**, the planar ligand structure of **ReL2** favors electron delocalization, thus rendering the rhenium(*i*) less electron rich and slightly decreasing the ease of its oxi-

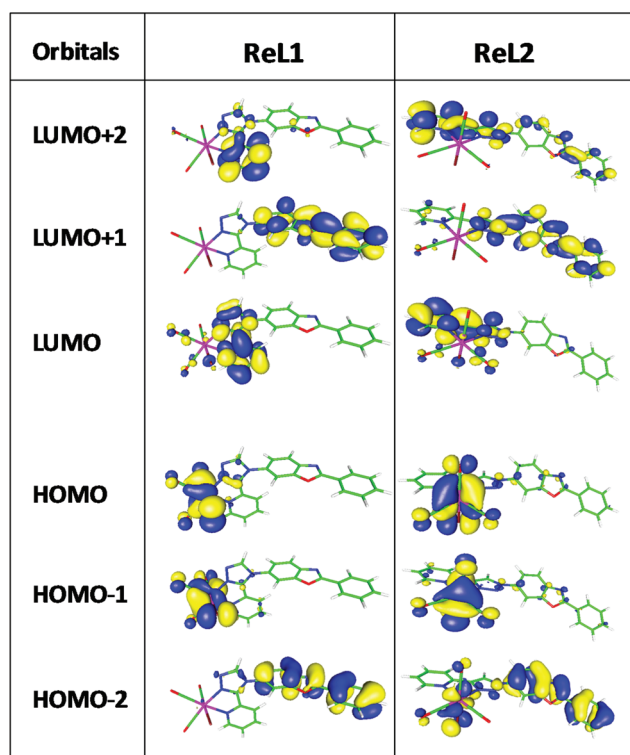


Fig. 3 Isodensity plots of selected frontier molecular orbitals involved in the first electronic transitions of **ReL1** and **ReL2** in DCM, according to TD-DFT calculations at the PBE1PBE/LANL2DZ/6-31+G** level of theory. Blue and yellow colors show regions of positive and negative spin density values, respectively.

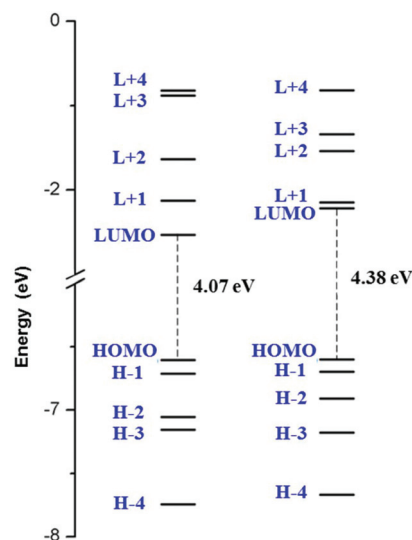


Fig. 4 Molecular orbital diagrams of **ReL1** (left) and **ReL2** (right).

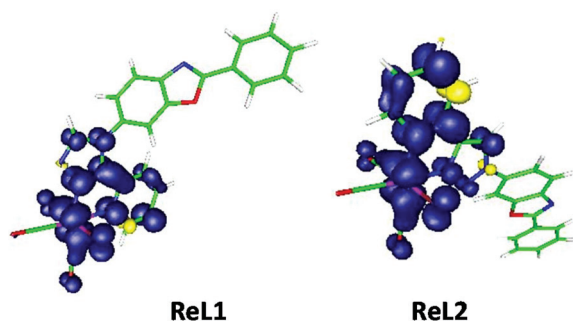


Fig. 5 Spin density distribution for the lowest triplet state T_1 of **ReL1** and **ReL2** in CH_2Cl_2 , according to a calculation based on the optimized triplet state with DFT method at the PBE1PBE/LanL2DZ level. Blue and yellow colors show regions of positive and negative spin density values, respectively.

Table 1 Selected electrochemical data of complexes **ReL1** and **ReL2** (6.5×10^{-3} M). Values determined by OSWV on a Pt working electrode in $\text{CH}_2\text{Cl}_2 + 0.1$ M $n[\text{Bu}_4\text{N}][\text{BF}_4]$ at room temperature.^{a,b} Ferrocene was used as internal reference

Compounds	Oxidation		Reduction	
	E_2	E_1	E_1	E_2
ReL1	+1.74	+1.44	-1.31	-1.90
ReL2	+1.79	+1.48	-1.60	-1.89

^a OSWVs were obtained using a sweep width of 20 mV, a frequency of 20 Hz, and a step potential of 5 mV. ^b Potential values in volts vs. SCE (Fc^+/Fc is observed at $0.55 \text{ V} \pm 0.01 \text{ V}$ vs. SCE).

dation. The reversibility of this process was not improved with a decrease or an increase in scan rate.

Considering now the cathodic part, both complexes presented a reduction process around -1.9 V (Fig. 6b) that is very likely attributed to the reduction of the PBO moiety of the ligand and confirms that the latter is not involved in the complexation process.²⁴ Indeed, a similar reduction process was detected for both ligands (Fig. S4[†]) and was also clearly visible in cyclic voltammetry (Fig. S5[†]). Another reduction process appeared at more anodic potential. In a first approach, it could be attributed to the reduction process of the substituted triazole ring whose potential value may substantially decrease by complexation as observed in related compounds.^{12,21,23,25} Remarkably, the value of the latter reduction potential strongly differed by more than 300 mV between the two compounds, *i.e.* -1.30 V for complex **ReL1** and -1.60 V for complex **ReL2**. These trends are well supported by the fact that the first calculated LUMO energy level implying the pyta (π^*) moiety is lower for **ReL1** (-2.53 eV) than for **ReL2** (-2.23 eV). Electrochemical HOMO–LUMO gap values (E_{gel})²⁶ found for complexes **ReL1** and **ReL2**, *i.e.* 2.55 and 2.85 eV respectively, fit very well with the calculated gap values 2.71 and 3.01 eV, highlighting good correlations with theoretical studies (see Table S14[†]).

Interestingly, the thorough examination of the first reduction process of the Re complexes at different scan rates

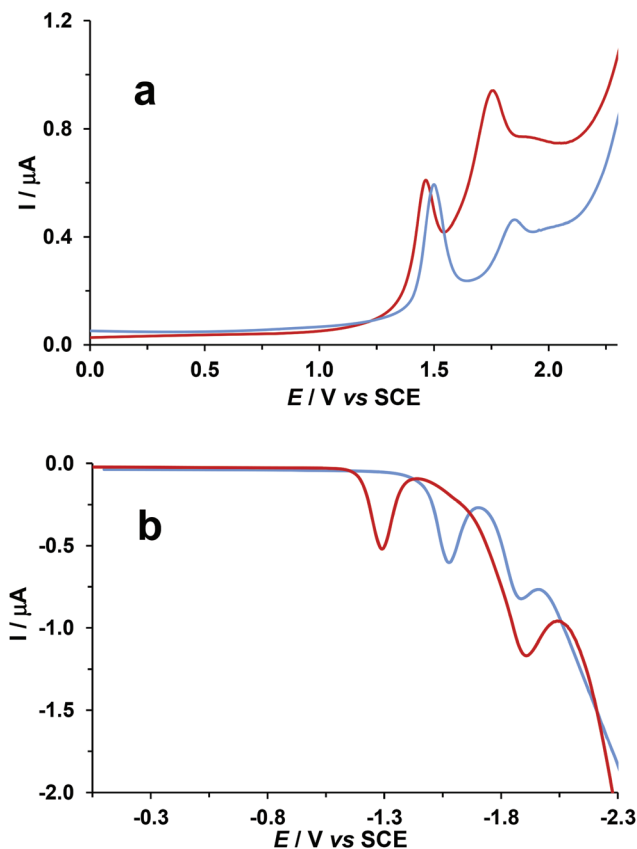


Fig. 6 OSWVs: anodic (a) and cathodic (b) scans of complexes **ReL1** (red) and **ReL2** (blue) on a Pt working electrode in $\text{CH}_2\text{Cl}_2 + 0.1$ M $n[\text{Bu}_4\text{N}][\text{BF}_4]$ at room temperature (frequency 20 Hz, amplitude 20 mV, step potential 5 mV).

showed that this process becomes quasi-reversible around 1 V s^{-1} only in the case of compound **ReL1** (Fig. S6[†]). This property is rather uncommon as this process is generally irreversible when implying the pyta moiety. It is noteworthy that, in cyclic voltammetry, a 1/1 intensity ratio was clearly observed between the first one-electron reduction process and the first one-electron oxidation process of compound **ReL2** (Fig. S7[†]). The use of a glassy carbon electrode allowed us to highlight the same phenomenon for compound **ReL1** (Fig. S8[†]).

To sum up, when comparing both complexes, the two main characteristic features are a significantly lower electrochemical gap for compound **ReL1** than for compound **ReL2**, and a different electrochemical behavior regarding the first reduction process. The latter property is probably related to the different nature of the two compounds. For compound **ReL2**, the LUMO and LUMO+1 energy levels are close: 0.07 eV (around 70 mV). Consequently, the first reduction potential detected at -1.60 V probably originates from the contribution of both the LUMO and LUMO+1 energy levels involving respectively the π^* (pyta) and $\pi^*(\text{pyta}) + \pi^*(\text{PBO})$ orbitals. In contrast for **ReL1**, the energy difference between these levels is greater (0.41 eV) and allows an easier electrochemical assignment of this reduction process exclusively resulting from the $\pi^*(\text{pyta})$ moiety.

Spectroscopic properties in solution

The spectroscopic properties of the two compounds in solution have been studied in three organic solvents of various polarity and proticity, *i.e.* DCM, acetonitrile and methanol. However, emphasis is given to results obtained in DCM for the sake of homogeneity with calculations and electrochemistry, and because these results are representative of the main behavior of our compounds. Solutions in DCM were perfectly stable at least for 24 h, and no aggregation was detected by UV-vis absorption spectroscopy in the investigated range of concentrations, *i.e.* below 2.6×10^{-4} M. It was checked by HPLC that the samples contained no traces of free ligands. All measurements were conducted in aerated solutions. Bubbling with argon led to an increase of the emission band intensity lower or equal to 15%, whatever the band considered. Table S15† collects the data in the three organic solvents, Table 2 presents selected data in DCM.

As illustrated in Fig. S9,† the experimental UV-vis absorption spectra of both complexes shown in Fig. 7 were in very good agreement with calculated spectra. The assignment of wavelengths was made on the basis of TD-DFT calculations (Tables S10 and S11†). Solutions of **ReL1** in DCM were bright yellow. The experimental absorption spectrum clearly showed a main band situated around 296 nm and a distinct low-intensity band peaking at 384 nm and tailing up to 450 nm (Fig. 7, top). The main band can be attributed to the $S_0 \rightarrow S_8$ and $S_0 \rightarrow S_9$ transitions with intra-ligand (IL) and metal-to-ligand charge transfer (MLCT) character, calculated at around 292 nm, and to the weak $S_0 \rightarrow S_6$ transition calculated at 300.9 nm. The long-wavelength band, typically observed in rhenium(i) tricarbonyl diimine complexes $[\text{ReX}(\text{CO})_3(\alpha, \alpha\text{-diimine})]$,^{4,6,27} clearly results here from a $S_0 \rightarrow S_2$ transition (at 378.4 nm), which involves the HOMO-1 and the LUMO and has strong MLCT character.

Solutions of complex **ReL2** were pale yellow. The absorption spectrum showed an intense band at 309 nm that smoothly extended above 400 nm (Fig. 7, bottom). The molar absorption coefficient was a little higher than for **ReL1** and this is in line with better electron delocalization. Most likely, the main band arises from the $S_0 \rightarrow S_6$, $S_0 \rightarrow S_5$ and $S_0 \rightarrow S_3$ transitions with MLCT and ligand-to-ligand charge transfer (ILCT) character, predicted to take place at 304.1 nm, 316.4 and 324.4 nm,

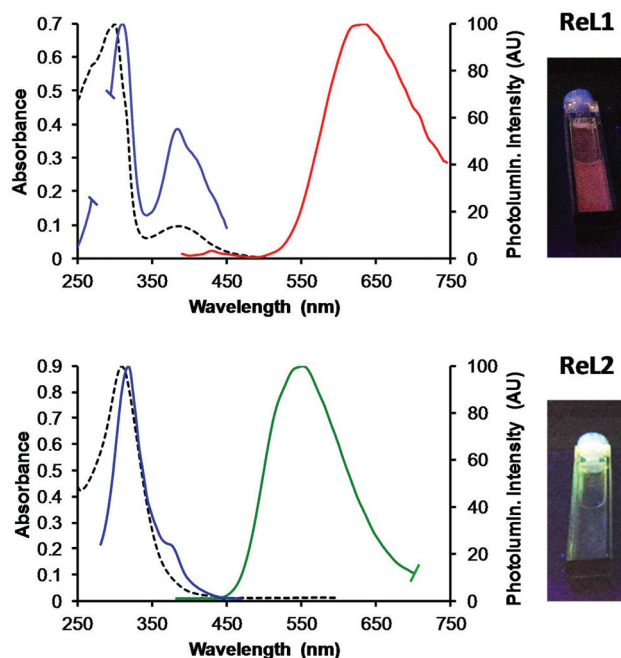


Fig. 7 Spectra of complex **ReL1** (top) and **ReL2** (bottom) in DCM. Absorption spectra (black dotted lines); normalized excitation spectra (blue lines) recorded at 560 nm and 540 nm, respectively; normalized emission spectra (red and green lines) upon excitation at 380 nm. Harmonic bands have been deleted for the sake of clarity. Complex concentration between 2.5×10^{-5} M and 1.5×10^{-5} M. Insets: Solutions illuminated by a UV lamp at 365 nm.

respectively. The absorption tail mainly arises from the weak $S_0 \rightarrow S_2$ transition, expected at 347.4 nm, which in this case does not generate a distinct MLCT band.

Upon excitation at 365 nm by a hand-held UV lamp, solutions of **ReL1** emitted red light detectable by the naked eye (inset of Fig. 7, top). The corresponding emission spectrum showed an intense band centered at around 628 nm and easily attributed to phosphorescence, which is expected at 645.1 nm for emission coming from the first triplet state (Table S13†). By comparison with the UV-absorption spectrum, the excitation spectrum showed strong contribution of the MLCT band, suggesting that excitation in this band favors phosphorescence emission. The phosphorescence quantum yield Φ_p was around

Table 2 Spectroscopic data of the complexes in dichloromethane and in the solid state (powder). Maximum absorption wavelength (λ_{abs}), molar extinction coefficient (ϵ), excitation wavelength (λ_{ex}), emission wavelength (λ_{em}), maximum wavelength of phosphorescence (λ_p) and photoluminescence (λ_{PL}) emission, phosphorescence and photoluminescence quantum yields (Φ_p and Φ_{PL} , respectively), luminescence decay time (τ). The concentration of complexes in solution was between to 2.5×10^{-5} M and 1.5×10^{-5} M

	Dichloromethane solution					Solid state		
	λ_{abs} (nm)	ϵ ($\text{M}^{-1} \text{cm}^{-1}$)	λ_p (nm)	Φ_p	τ (ns)	λ_{PL} (nm)	Φ_{PL}	τ (ns)
ReL1	296, 384	27 800, 3900	628	0.017	74.7 ^a	584, 622	0.065	338 ^b
ReL2	309	34 100	546	0.015	192 ^c	542	0.016	414 ^d

If not specified, excitation was performed at 380 nm. ^a $\lambda_{\text{ex}} = 330$ nm, $\lambda_{\text{em}} = 560\text{--}720$ nm. ^b $\lambda_{\text{em}} = 560\text{--}690$ nm. ^c $\lambda_{\text{em}} = 500\text{--}630$ nm. ^d $\lambda_{\text{em}} = 490\text{--}640$ nm.

0.017. The emission decay was almost monoexponential with a long lifetime of 74.7 ns, totally in line with phosphorescence emission (Fig. S10†).

Solutions of complex **ReL2** emitted green light upon excitation with the UV lamp (inset of Fig. 7, bottom). The emission spectrum was dominated by a strong band with maximum at 546 nm, close to the value calculated for phosphorescence emission (553.2 nm). The corresponding excitation spectrum was close to the absorption spectrum, except for a little band around 370 nm, *i.e.* in the MLCT region. Like for the former complex, albeit to a lesser extent, it seems that excitation in this region promotes phosphorescence emission. The phosphorescence quantum yield was 0.015. The decay was monoexponential with a lifetime value of 192 ns (Fig. S10†).

In summary, both complexes share some common spectroscopic features in solution. In particular, they exhibit phosphorescence in solution at room temperature, as commonly observed for tricarbonyl Re(i) complexes,^{1–9} in which strong spin-orbit coupling promotes efficient intersystem crossing (ISC) between singlet and triplet manifolds. The most striking difference is that the phosphorescence emission of **ReL1** was red-shifted by 82 nm with respect to **ReL2**. Though moderate, the phosphorescence quantum yields of these compounds compare well with those of many rhenium complexes used for bio-imaging in the literature.^{3–5} It is also noteworthy that their phosphorescence intensity was reduced with increasing the polarity and proticity of the solvent (Table S15†). This effect was moderate for **ReL1** and particularly strong for **ReL2**, for which emission was almost no detectable in methanol. It is reminiscent of the total phosphorescence quenching observed in the presence of water for Re(i) tricarbonyl complexes possessing a pyta fragment, where the 1,2,3-triazole unit is functionalized by an aliphatic substituent.⁷

To get a clear overview of the photophysical behavior in solution, the energy diagrams are presented in Fig. 8. In the absence of ultra-fast spectroscopy measurements, we cannot

comment on possible $S_m \rightarrow T_m$ ($m > 1$) ISC. For the sake of simplicity, it was assumed that high-energy singlet states deactivate to the S_1 *via* internal conversion (IC), and S_1 subsequently decays to the lowest triplet state T_1 that is responsible for phosphorescence. The diagram takes into account the observation that excitation to higher electronic excited states contributes less to phosphorescence emission than excitation in the MLCT band, as already reported in the literature.²⁸ An explanation is that S_2 , S_1 and T_1 involve orbitals with close electron distribution, and so ISC may be facilitated by the small electron reorganization required. In contrast, high-energy excited states, which involve different types of orbitals, may undergo easy radiationless pathways down to the ground state. The behavior of the complexes could thus be explained by small differences in their photophysical processes. According to Table S12,† for **ReL1**, the S_2 excited state is almost the only excited state involved in the emission process with a significant oscillator strength (0.1748), so it could be the most important intermediate in collecting the emission energy, while for **ReL2**, the S_3 and S_4 states that have significant f values could also play an active role.

Spectroscopic properties in the solid state

Notably, the solid complex **ReL1** strongly emitted yellow light, while **ReL2** emitted green light (Fig. 9, insets). The spectroscopic behavior of the two complexes in pristine powder form was thus investigated using an integrating sphere. For **ReL1**, the emission spectrum exhibited two maxima at 584 and 622 nm (Fig. 9). The long wavelength band is reminiscent of that observed in solution at 628 nm. For **ReL2**, the spectrum was centered on 542 nm, very close from that of solutions.

Long decay times of 338 ns and 414 ns were predominant for **ReL1** and **ReL2**, respectively (Table S16 and Fig. S11†), confirming that the nature of solid-state emission is mainly phosphorescence. The lifetimes have been markedly increased with passing from solutions to the solid state, and this stabilization effect is more pronounced for **ReL1** than for **ReL2**. The photoluminescence quantum yields Φ_{PL} of **ReL1** and **ReL2** were

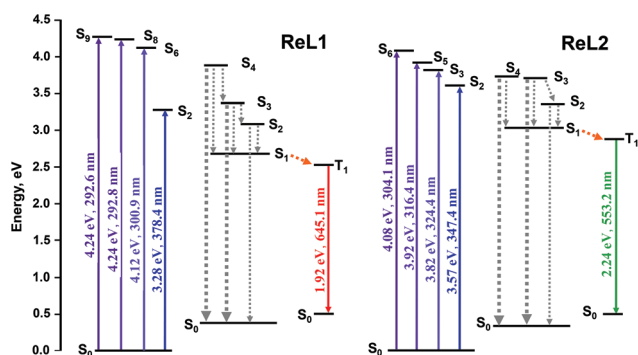


Fig. 8 Simplified schematic energy level diagram describing the main photophysical processes of complexes **ReL1** and **ReL2** in DCM solution, in optimized ground state, first singlet excited state and first triplet excited state geometry (from left to right for each complex). Radiative transitions are in colored solid lines, internal conversion (IC) in grey dotted lines, intersystem crossing (ISC) in orange dotted lines. $S_m \rightarrow T_m$ ($m > 1$) intersystem crossing not represented.

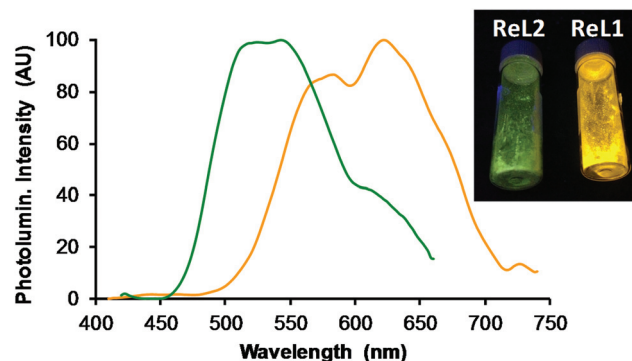


Fig. 9 Normalized emission spectra of complexes **ReL1** (orange line) and **ReL2** (green line) in the solid state (pristine powders) upon excitation at 380 nm. Inset: Picture of the complexes as powders under illumination by a UV lamp, $\lambda_{ex} = 365$ nm.

0.065 and 0.016, respectively (Table 2). The comparison with the corresponding Φ_p values in solution shows that the whole emission intensity is the same for **ReL2**, yet multiplied by 3.8 for **ReL1**. The latter phenomenon can be related to an increase of phosphorescence emission upon aggregation (AIPE).^{29,30} For our compounds, the decrease of phosphorescence intensity induced by water prevents us from making the popular demonstration of AIPE behavior, which consists in adding water to an organic solution of dye to promote aggregation and to visualize the associated emission enhancement. However, the comparison of the solution and solid-state quantum yields speaks for itself. The different behavior of both complexes may be easily understood. Indeed, the π - π stacking interactions that take place between the aromatic rings of **ReL2** lead to intermolecular quenching, which is detrimental to the emission of light in the solid state. In contrast, the bent conformation of **ReL1** prevents π - π stacking, and thus promotes light emission.²⁹ In parallel, the intramolecular rotations between the pyta and PBO groups are restricted like other possible molecular motions, reducing non emissive deactivation pathways. These combined effects are mostly responsible for the observed AIPE effect.³⁰ So, the peculiar conformation of **ReL1** plays a key role regarding the emission properties.

It must be kept in mind that the solid-state characteristics reported here only refer to the investigated powders. Indeed, other values could have been found with single crystals or with powders prepared from recrystallization in other solvents, as it is well known that the molecular arrangement and surface defects play an essential role in solid-state properties.³¹

Conclusions

For a long time, various triazole groups have been prepared *via* click chemistry or conventional synthesis to play the role of linkers or to be part of the coordinating agent of transition metal complexes,¹¹ as it is the case for pyta ligands. However, except for some complexes, the importance of the nature of the triazole group has attracted little interest.^{12,13} Remarkably, the present work revealed that the triazole isomerism impacts the properties of the corresponding complexes, at least in the particular case where the triazole group bears a PBO moiety. For instance, with the 1,2,4-triazole isomer like in **ReL1**, steric hindrance occurs due to the proximity of PBO with the pyridyl group. The PBO moiety is then positioned out of plane and behaves more independently from an electronic point of view. Electron delocalization is better in **ReL2** that incorporates a planar organic fragment. However, this difference between complexes does not account for all the experimental results. For example, intuitively, it might have been expected that **ReL2** emits at longer wavelengths than **ReL1**, and this is not the case.

To better understand what occurs, it is instructive to compare **ReL2** with closely related tricarbonyl Re(i) complexes reported in the literature. Complexes that incorporate a pyta group in which the 1,2,3-triazole moiety is substituted by an alkyl substituent on the N(1) nitrogen atom emit phosphor-

escence at rather short wavelengths (around 522–528 nm) in organic solvents.^{7,22b} After substitution by a phenyl group, the emission maximum is around 538–543 nm.^{20,22a} In the case of **ReL2**, grafting of the electron-withdrawing PBO group to the 1,2,3-triazole moiety moderately shifts the emission spectra till 546 nm in solution. Above all, the presence of the PBO group induces an enhancement of the phosphorescence quantum yield by one order of magnitude. By this respect, complexes are thus a little sensitive to the nature of the substituent borne by the 1,2,3-triazole moiety, although it has been shown for other metal complexes that this moiety generally behaves as an insulator.^{12,21,32}

No direct comparison can be made for **ReL1** because this substitution pattern has not been investigated in the literature. However, it is obvious that **ReL1** emits at much longer wavelengths than pyta-based complexes possessing a 1,2,3-triazole moiety. Most importantly, our TD-DFT calculations pointed out a smaller HOMO–LUMO energy gap in **ReL1** than in **ReL2**, which is in line with the lower first electrochemical reduction potential and the red-shift of the phosphorescence spectrum observed for the former complex. This difference is certainly related to the intrinsic electron properties of the complexes, due to the very nature of the triazole group. It is noteworthy that the HOMO and LUMO of both **ReL1** and **ReL2** are exclusively centered around the metal and the pyta group, with little involvement of the PBO moiety. The comparison with other molecules would allow determining the exact role played by the substituent in the HOMO–LUMO energy levels.

Remarkably, the presence of the PBO group plays a crucial role in the solid-state emission properties. Here, it led to complexes that emit light in the solid state at least with the same efficiency as in solution. At the moment, **ReL1** is the first mononuclear Re(i) complex reported to exhibit AIPE behavior,³⁰ and this property is obviously due to its bent geometry that results from the presence of PBO on the 1,2,4-triazole group. The development of Re(i) complexes based on this framework is presently underway in our laboratory with the aim of improving the solid-state luminescence properties.

To sum up, this work showed that triazole-based complexes must be carefully designed depending on the envisaged applications. The 1,2,4-triazole isomer deserves being more widely used, and substitution on the N(4) nitrogen atom by an aromatic fragment with extended π -electron conjugation is probably a distinct advantage, as far as solid-state luminescence properties are desired. Using the synthetic strategy described above, various organic dyes could be combined with the triazole fragment to modulate the spectroscopic and photophysical behavior of the desired complexes. Following this approach should provide precious data to better rationalize the design of highly emissive and specific Re(i) luminescent materials.

Experimental section

All purchased chemicals were of the highest purity commercially available and used without further purification.

Analytical grade solvents were used and not further purified unless specified. Reactions were monitored by analytical thin layer chromatography (TLC) on Kieselgel 60 F254 (Merck). Chromatography purification was conducted using silica gel or neutral alumina obtained from Merck. NMR, mass and infrared spectra were obtained in the relevant 'Services communs de l'Institut de Chimie de Toulouse, Université de Toulouse III-Paul-Sabatier'. ^1H - and ^{13}C -NMR spectra were measured with Bruker Avance DRX 500 MHz or Bruker Avance 300 MHz. Attributions of the signals were made using 2D NMR data (COSY, HSQC and HMBC). For ligands and complexes, protons and carbon atoms were numbered according to Fig. S12.† Electro spray mass spectra were obtained using a QTRAP Applied Biosystems spectrometer and high-resolution mass spectra (HRMS) were recorded using an LCT Premier Waters spectrometer. Desorption chemical ionization (DCI) mass spectra (NH_3 or CH_4) were obtained on a DSQ II Thermofisher apparatus. Infrared spectra were obtained on a Nexus Thermo Nicolet apparatus with DTGS as the detector. The microanalyses were performed with a PerkinElmer 2400 elemental analyzer in the 'Service d'Analyse Chimique du Laboratoire de Chimie de Coordination de Toulouse' (LCC, Toulouse). The compound purity was checked by HPLC, using an Acquity CSH C18 column and a water/acetonitrile gradient as the eluent. Detection was made with MS, absorption and fluorescence detectors.

General procedure for the preparation of ligands

6-Nitro-2-phenylbenzoxazole (1). The mixture of 2-amino-5-nitrophenol (10 mmol, 1.54 g), benzoic acid (10 mmol, 1.22 g) and polyphosphoric acid (24 g) was heated to 110 °C with stirring for 16 h. After reaction, iced water (100 mL) was added. The resulting mixture was neutralized with 10% NaOH solution and extracted with ethyl acetate (3 × 60 mL). All organic layers were combined, washed with water, dried over anhydrous MgSO_4 , filtered and concentrated to dry. The residue was purified by column chromatography using ethyl acetate/petroleum ether (v/v = 1/5) as eluent to obtain 1.91 g of yellow solid, yield 80%. ^1H NMR (300 MHz, CDCl_3): δ (ppm) = 8.48 (dd, J = 0.5 Hz, J = 2.2 Hz, 1H, ArH), 8.33–8.26 (m, 3H, ArH), 7.83 (dd, J = 0.5 Hz, J = 8.8 Hz, 1H, ArH), 7.65–7.53 (m, 3H, ArH). DCI-MS (CH_4): m/z calcd for $\text{C}_{13}\text{H}_9\text{N}_2\text{O}_3^+$: 241.0608 [$\text{M} + \text{H}$] $^+$; found: 241.0607.

6-Amino-2-phenylbenzoxazole (2). To a solution of **1** (1.07 g, 4.5 mmol) in $\text{MeOH}/\text{CHCl}_3$ (1 : 2 v/v, 30 mL) was added 10% Pd/C (0.33 g). The mixture was carried out under 6 bars pressure of H_2 and stirred at room temperature for 24 h. After reaction, the mixture was filtered twice to remove the catalyst. The filtrate was concentrated to dry and purified by column chromatography using DCM as eluent to obtain 0.82 g of pale white solid, yield 87%. ^1H NMR (300 MHz, CDCl_3): δ (ppm) = 8.20–8.16 (m, 2H, ArH), 7.54–7.48 (m, 4H, ArH), 6.88 (d, J = 2.2 Hz, 1H, ArH), 6.70 (dd, J = 2.1 Hz, J = 8.4 Hz, 1H, ArH). DCI MS (NH_3): m/z calcd for $\text{C}_{13}\text{H}_{11}\text{N}_2\text{O}^+$: 211.1 [$\text{M} + \text{H}$] $^+$; found: 211.0.

6-Azido-2-phenylbenzoxazole (3). To an aqueous solution of HCl (6 N, 20 mL), compound **2** (420 mg, 2 mmol) was added at

0–4 °C with stirring, then extra ethanol was added until the solid dissolved completely. Then, sodium nitrite (262 mg, 3.8 mmol) in water was added dropwise and the mixture was stirred at 0–4 °C for 45 min. Sodium azide (195 mg, 3 mmol) was added slowly. The mixture was stirred for another 2 h and extracted with diethyl ether (50 mL × 3). All the organic layers were combined, washed with saturated NaHCO_3 aqueous solution (50 mL × 2), dried over anhydrous MgSO_4 , filtered and concentrated to dry. The residue was dried under vacuum without further purification to afford 405 mg of yellow solid, yield 86%. ^1H NMR (300 MHz, CDCl_3): δ (ppm) = 7.04 (dd, J = 2.1 Hz, J = 8.5 Hz, 1H, ArH), 7.27 (dd, J = 0.5 Hz, J = 2.1 Hz, 1H, ArH), 7.53–7.53 (m, 3H, ArH), 7.72 (dd, J = 0.5 Hz, J = 8.5 Hz, 1H, ArH), 8.21–8.24 (m, 2H, ArH). DCI MS (NH_3): m/z calcd for $\text{C}_{13}\text{H}_9\text{N}_4\text{O}^+$ [$\text{M} + \text{H}$] $^+$: 237.1; found: 237.0. IR: $\nu_{(\text{N}_3)}$ = 2113 cm^{-1} .

2-Phenyl-6-(3-(pyridin-2-yl)-4H-1,2,4-triazol-4-yl)benzoxazole (L1). To a solution of pyridine-2-carbohydrazide (287 mg, 2.1 mmol) in distilled CH_3CN (5 mL), *N,N*-dimethylformamide dimethyl acetal (250 mg, 2.1 mmol) was added dropwise under argon. The mixture was heated to 50 °C with stirring for 3 h and then **2** (400 mg, 1.9 mmol) in CH_3CN (15 mL) was added as well as acetic acid (3 mL). The mixture was heated to 120 °C for 16 h. After cooling to room temperature, the mixture was filtered and the precipitate was washed with diethyl ether. The residue was purified on column chromatography using MeOH/DCM (1 : 10 v/v) as eluent to afford 200 mg of light yellow solid, yield 31%. ^1H NMR (500 MHz, $\text{DMSO}-d_6$): δ (ppm) = 8.97 (s, 1H, H_5), 8.35 (ddd, J = 4.9, 1.8, 0.9 Hz, 1H, H_6), 8.28–8.16 (m, 2H, $\text{H}_{b,f}$), 8.10 (dt, J = 7.9, 1.1 Hz, 1H, H_3), 8.02 (d, J = 2.0 Hz, 1H, H_7), 7.97 (td, J = 7.8, 1.8 Hz, 1H, H_4), 7.88 (d, J = 8.4 Hz, 1H, H_4), 7.71–7.60 (m, 3H, $\text{H}_{c,d,e}$), 7.41 (ddd, J = 8.6, 5.2, 1.7 Hz, 2H, $\text{H}_{5,5'}$). ^{13}C NMR (125 MHz, $\text{DMSO}-d_6$): δ (ppm) = 164.3 (C_2), 152.1 (C_2'), 150.2 (C_8), 149.5 (C_6), 147.1 (C_5), 146.9 (C_3), 142.0 (C_6), 137.8 (C_4'), 133.0 (C_9), 132.9 (C_d), 129.9 ($\text{C}_{c,e}$), 127.9 ($\text{C}_{b,f}$), 126.5 (C_a), 125.0 ($\text{C}_{5'}$), 124.4 (C_3), 124.0 (C_5), 120.1 (C_4), 110.0 (C_7). ESI-HRMS: m/z calcd for $\text{C}_{20}\text{H}_{14}\text{N}_5\text{O}^+$: 340.1198 [$\text{M} + \text{H}$] $^+$, found 340.1195. Anal. calcd (%) for $\text{C}_{20}\text{H}_{13}\text{N}_5\text{O}$: C 70.79, H 3.86, N 20.64; found: C 70.51, H 3.63, N 20.79.

2-Phenyl-6-(4-(pyridin-2-yl)-1H-1,2,3-triazol-1-yl)benzoxazole (L2). A mixture of 2-ethynylpyridine (103 mg, 1 mmol), 6-azido-2-phenylbenzoxazole (**3**) (260 mg, 1.1 mmol), copper(II) acetate monohydrate (60 mg, 0.3 mmol) and sodium ascorbate (100 mg, 0.5 mmol) in acetonitrile (20 mL) was stirred at room temperature for 16 h. The resulting mixture was evaporated to remove the solvent and then dissolved in DCM (50 mL), washed with saturated Na_2EDTA solution (30 mL × 2), dried with anhydrous MgSO_4 and filtered. The filtrate was evaporated and recrystallized with DCM and diethyl ether to afford 225 mg of pale solid, yield 66%. ^1H NMR (500 MHz, $\text{DMSO}-d_6$): δ (ppm) = 9.44 (s, 1H, H_5), 8.69 (m, 1H, H_6), 8.53 (d, J = 2.1 Hz, 1H, H_7), 8.26–8.24 (m, 2H, $\text{H}_{b,f}$), 8.16–8.12 (m, 2H, $\text{H}_{4,5}$), 8.05 (d, J = 8.6 Hz, 1H, H_3), 7.99–7.96 (m, 1H, H_4), 7.70–7.64 (m, 3H, $\text{H}_{c,d,e}$), 7.44–7.42 (m, 1H, H_5). ^{13}C NMR (125 MHz, $\text{DMSO}-d_6$): δ (ppm) = 164.4 (C_2), 150.9 (C_2'), 150.2 (C_6), 149.9 (C_8), 148.8 (C_6), 142.1 (C_9), 137.8 (C_4'), 134.5 (C_4),

132.9 (C_d), 129.9 (C_{c,e}), 128.0 (C_{b,f}), 126.5 (C_a), 123.5 (C_{5'}), 122.2(C₅), 121.1 (C_{3'}), 120.3 (C₅), 118.1 (C₄), 104.2 (C₇). ESI-HRMS: *m/z* calcd for C₂₀H₁₄N₅O⁺: 340.1198 [M + H]⁺; found: 340.1197; *m/z* calcd for C₂₀H₁₃N₅ONa⁺: 362.1018 [M + Na]⁺; found 362.1015. Anal. calcd (%) for C₂₀H₁₃N₅O: C 70.79, H 3.86, N 20.64; found: C 70.49, H 3.69, N 20.52.

General procedure for the preparation of tricarbonyl rhenium(i) complexes

A mixture of ligand and [Re(CO)₅Cl] (1.15 eq.) in methanol was stirred overnight at 65 °C. After consumption of the ligand, the mixture was cooled to room temperature and filtered, the precipitate was purified by chromatography on silica gel using ethylacetate as eluent to afford the desired product.

ReL1. 50 mg (0.15 mmol) of **L1** and 58 mg (0.16 mmol) of [Re(CO)₅Cl] afforded 65 mg of the complex **ReL1** as a yellow solid. Yield: 67%. ¹H NMR (500 MHz, DMSO-*d*₆): δ (ppm) = 9.31 (s, 1H, H_{5'}), 9.17–9.06 (m, 1H, H_{6'}), 8.47 (s, 1H, H₇), 8.35–8.21 (m, 2H, H_{b,f}), 8.15 (d, *J* = 8.4 Hz, 1H, H_d), 8.04 (td, *J* = 8.0, 1.5 Hz, 1H, H_{4'}), 7.84–7.55 (m, 5H, H_{c,e,4,5,5'}), 7.21 (dd, *J* = 8.1, 1.1 Hz, 1H, H_{3'}). ¹³C NMR (125 MHz, DMSO-*d*₆): δ (ppm) = 198.3, 197.7, 189.5 (C≡O), 165.4 (C₂), 155.1 (C₃), 155.0 (C_{6'}), 150.8 (C₈), 148.9 (C₅), 144.5 (C_{2'}), 144.2 (C₉), 141.2 (C_{4'}), 133.3 (C₅), 130.0 (C_{c,e}), 129.3 (C₆), 128.8 (C_{5'}), 128.2 (C_{b,f}), 126.2 (C_a), 124.7 (C₄), 123.8 (C_{3'}), 121.7 (C_d), 111.4 (C₇). ESI-HRMS: *m/z* calcd for C₂₃H₁₃N₅O₄Cl¹⁸⁵ReNa⁺: 666.0083 [M + Na]⁺; found 666.0096; *m/z* calcd for C₂₃H₁₃N₅O₄¹⁸⁵Re⁺: 608.0497 [M – Cl]⁺; found: 608.0510. Anal. calcd (%) for C₂₃H₁₃N₅O₄ReCl: C 42.83, H 2.03, N 10.86; found: C 42.59, H 1.92, N 10.67. IR: ν(C≡O) = 2025, 1919, 1884 cm⁻¹.

ReL2. 100 mg (0.30 mmol) of **L2** and 123 mg (0.34 mmol) of [Re(CO)₅Cl] afford 130 mg of complex **ReL2** as pale yellow solid. Yield: 68%. ¹H NMR (500 MHz, DMSO): δ (ppm) = 10.04 (s, 1H, H₅), 9.05 (ddd, *J* = 5.1, 1.8, 0.8 Hz, 1H, H_{6'}), 8.57 (dd, *J* = 2.1, 0.5 Hz, 1H, H₇), 8.39 (td, *J* = 7.9, 1.5 Hz, 1H, H_{4'}), 8.33–8.27 (m, 3H, H_{b,f,3'}), 8.15 (dd, *J* = 8.6, 0.5 Hz, 1H, H₅), 8.10 (dd, *J* = 8.6, 2.1 Hz, 1H, H₄), 7.74–7.67 (m, 4H, H_{c,d,e,5'}). ¹³C NMR (125 MHz, DMSO): δ (ppm) = 198.0, 197.1, 190.0 (C≡O), 165.2 (C₂), 153.7 (C_{6'}), 150.8 (C_{2'}), 149.6 (C₈), 148.9 (C₆), 143.4 (C₉), 141.4 (C_{4'}), 133.2 (C_d), 133.1 (C₄), 130.0 (C_{c,e}), 128.1 (C_{b,f}), 127.3 (C_{5'}), 126.3 (C_a), 125.4 (C₅), 123.2 (C_{3'}), 121.5 (C₅), 119.1 (C₄), 105.5 (C₇). ESI-HRMS: *m/z* calcd for C₂₃H₁₃N₅O₄Cl¹⁸⁵ReNa⁺: 666.0083 [M + Na]⁺, found 666.0099; *m/z* calcd for C₂₃H₁₃N₅O₄¹⁸⁵Re⁺: 608.0497 [M – Cl]⁺, found 608.0513. Anal. calcd (%) for C₂₃H₁₃N₅O₄ReCl: C 42.83, H 2.03, N 10.86; found: C 43.15, H 2.21, N 11.18. IR: ν(C≡O) = 2030, 1920, 1903 cm⁻¹.

X-ray crystallography

X-Ray quality crystals of **ReL1** were obtained by diffusion crystallization of CH₃CN and diethyl ether. Single crystals of **ReL2** and **L2** were slowly grown in acetone and DCM, respectively. Crystal data were collected on a Bruker AXS Quazar APEX II diffractometer using a 30 W air-cooled microfocus source (ImS) with focusing multilayer optics using MoK α radiation (wavelength = 0.71073 Å). Phi- and omega-scans were used.

The structures were solved by direct methods (SHELXS 97) or using intrinsic phasing method (ShelXT).^{33,34} All non-hydrogen atoms were refined anisotropically using the least-square method on *F*².³⁴ Full crystallographic data are collected in Table S1.†

Computational details

The GAUSSIAN09 program package³⁵ was employed for all calculations (the geometry optimization, the ground-state and excited-state electronic structures, and optical spectra) with the aid of the ChemCraft visualization program.³⁶ The ground state (S₀), the first excited state (S₁) and the lowest triplet state (T₁) geometries of compounds were fully optimized with the restricted and unrestricted density functional theory (R-DFT and U-DFT) method using the Perdew–Burke–Ernzerhof PBE1PBE functional without symmetry constraints.³⁷ In all calculations, the “double- ζ ” quality basis set LANL2DZ with Hay and Wadt’s relative effective core potential ECP (outer-core [[5s25p6]] electrons and the (5d6) valence electrons)³⁸ was employed for the Re atom. The 6-31+g** basis set for H, C, N, O and Cl atoms was used.³⁹ The vibrational frequencies calculations were performed using the optimized structural parameters of compounds, to confirm that each optimized structure represents a local minimum on the potential energy surface and all eigenvalues are non-negative. The optimized Cartesian coordinates of compounds are included in the ESI part (Tables S17 and S18†). On the basis of the optimized ground and excited state geometries, the absorption and emission properties were calculated by the time dependent density functional theory (TD-DFT) method at the PBE1PBE/LANL2DZ/6-31+G** level. The solvent effect (DCM, ϵ = 9.08) was simulated using the Self-Consistent Reaction Field (SCRFF) under the Polarizable Continuum Model (PCM).⁴⁰ These methods have already shown good agreement with experimental studies for different rhenium(i) complexes.⁴¹

Electrochemistry

Osteryoung square wave voltammetry (OSWV) and cyclic voltammetry (CV) measurements were made in DCM at a ligand concentration of 3.4 × 10⁻³ M and a complex concentration of 6.5 × 10⁻³ M. The supporting electrolyte *n*[Bu₄N][BF₄] (Fluka, 99% electrochemical grade) was used as received and simply degassed under Ar. DCM was dried in an MB SPS-800 Solvent Purification System just prior to use. The measurements were carried out with a potentiostat Autolab PGSTAT100 controlled by GPES 4.09 software. Experiments were performed at room temperature (r.t.) in a homemade airtight three-electrode cell connected to a vacuum/Ar line. The reference electrode consisted of a saturated calomel electrode (SCE) separated from the solution by a bridge compartment. The counter electrode was a Pt wire of ca. 1 cm² apparent surface. The working electrode was a Pt microdisk (0.5 mm diameter). OSWV experiments were carried out at room temperature using a sweep width of 20 mV, a frequency of 20 Hz, and a step potential of 5 mV. Before each measurement, the solutions were degassed with Ar and the working electrode was polished with a polish-

ing machine (Presi P230). Ferrocene was used as internal reference (Fc + /Fc, 0.55 ± 0.01 V vs. SCE).

Spectroscopy and photophysics

Dye solutions were prepared by gentle heating in a solvent, sonication and filtration on paper filter prior to measurement. Spectroscopic measurements in solutions were conducted at 20 °C in a temperature-controlled cell. UV-visible absorption spectra were recorded on a Hewlett Packard 8453 spectrometer. Fluorescence spectra in solutions were measured with a Cary Eclipse spectrofluorometer and a Xenius SAFAS spectrofluorometer using cells of 1 cm optical pathway. All fluorescence spectra were corrected. The fluorescence quantum yields in solution (Φ_F) were determined using the classical formula: $\Phi_{Fx} = (A_s \times F_x \times n_x^2 \times \Phi_{Fs}) / (A_x \times F_s \times n_s^2)$ where A is the absorbance at the excitation wavelength, F the area under the fluorescence curve and n the refraction index. Subscripts s and x refer to the standard and to the sample of unknown quantum yield, respectively. Coumarin 153 in ethanol ($\Phi_F = 0.53$)⁴² was used as the standard for excitation at 380 nm. The absorbance of the solutions was equal or below 0.055 at the excitation wavelength. The error on the quantum yield values is estimated to be about 10%.

Solid state photoluminescence quantum yields were recorded on a SAFAS Xenius spectrofluorometer equipped with a BaSO₄ integrating sphere and a Hamamatsu R2658 detector. Solid samples were deposited on a metal support and luminescence spectra were corrected. The absolute photoluminescence quantum yield values (Φ_P) were determined by a method based on the one developed by De Mello *et al.*⁴³ The excitation source was scanned in order to evaluate the reflected light for the empty sphere (L_a), the samples facing the source light (L_c) and the sample out of the irradiation beam (L_b). The fluorescence spectra were recorded with the sample facing the source light (E_c) and out from the direct irradiation (E_b). The PM voltage was adapted to the measurement of reflected light and emission spectra, respectively, and proper correction was applied to take into account the voltage difference. The Φ_P values were then calculated using the formula:

$$\Phi_P = E_c - (1 - \alpha)E_b/L_a\alpha$$

with $\alpha = 1 - L_c/L_b$. The error was estimated to be about 20%.

Fluorescence decay curves were obtained by the time-correlated single-photon counting (TCSPC) method with a femtosecond laser excitation composed of a Titanium Sapphire laser (Tsunami, Spectra-Physics) pumped by a doubled Nd:YVO₄ laser (Millennia Xs, Spectra-Physics). Light pulses at 760 nm (resp. 900 nm, or 990 nm) from the oscillator were selected by an acousto-optic crystal at a repetition rate of 4 MHz, and then doubled at 380 nm (resp. tripled at 300 nm, or 330 nm) by non-linear crystals. Fluorescence photons were detected at 90°, through a polarizer at magic angle and a monochromator, by means of a Hamamatsu MCP R3809U photomultiplier, connected to a SPC-630 TCSPC module from Becker & Hickl. Large emission band-pass of the monochromator was set in order to optimize the count rate of the signal and allow good quality of

the data. The instrumental response function was recorded before each decay measurement with a full width at half-maximum (fwhm) of ~25 ps. The fluorescence data were analyzed using the Globals software package developed at the Laboratory for Fluorescence Dynamics at the University of Illinois at Urbana-Champaign, which includes reconvolution analysis and global non-linear least-squares minimization method.

Conflicts of interest

There are no conflict of interest to declare.

Acknowledgements

J. Wang thanks the Chinese Scholarship Council (CSC) for a Ph.D. funding. M. Wolff acknowledges financial support from the Foundation for Polish Science (START 2014). Calculations were carried out in Wroclaw Centre for Networking and Supercomputing, Poland (<http://www.wcss.pl>). We thank Dr A. Saquet and A. Moreau (LCC) for electrochemical measurements. We thank the Integrated Screening Platform of Toulouse (PICT IBIa) for providing access to HPLC equipment and Mrs I. Fabing for skilled help. We are also indebted to Prof. F. Alary (University of Toulouse III) for a fruitful discussion.

References

- 1 M. Wrighton and D. L. Morse, *J. Am. Chem. Soc.*, 1974, **96**, 998–1003.
- 2 (a) A. Kumar, S.-S. Sun and A. J. Lees, *Top. Organomet. Chem.*, 2010, **29**, 1–35; (b) A. Coleman, C. Brennan, J. G. Vos and M. T. Pryce, *Coord. Chem. Rev.*, 2008, **252**, 2585–2595; (c) R. A. Kirgan, B. P. Sullivan and D. P. Rillema, *Top. Curr. Chem.*, 2007, **281**, 45–100.
- 3 (a) L. C.-C. Lee, K.-K. Leung and K. K.-W. Lo, *Dalton Trans.*, 2017, **46**, 16357–16380; (b) K. K.-W. Lo, *Acc. Chem. Res.*, 2015, **48**, 2985–2995.
- 4 (a) A. J. Amoroso, R. J. Arthur, M. P. Coogan, J. B. Court, V. Fernández-Moreira, A. J. Hayes, D. Lloyd, C. Millet and S. J. A. Pope, *New J. Chem.*, 2008, **32**, 1097–1102; (b) A. J. Amoroso, M. P. Coogan, J. E. Dunne, V. Fernández-Moreira, J. B. Hess, A. J. Hayes, D. Lloyd, C. Millet, S. J. A. Pope and C. Williams, *Chem. Commun.*, 2007, 3066–3068; (c) L. Raszeja, A. Maghnouj, S. Hahn and N. Metzler-Nolte, *ChemBioChem*, 2011, **12**, 371–376; (d) K. Kowalski, Ł. Szczupak, T. Bernaś and R. Czerwieńiec, *J. Organomet. Chem.*, 2015, **782**, 124–130; (e) R. G. Balasingham, F. L. Thorp-Greenwood, C. F. Williams, M. P. Coogan and S. J. A. Pope, *Inorg. Chem.*, 2012, **51**, 1419–1426; (f) M.-W. Louie, A. W. T. Choi, H. W. Liu, B. T. N. Chan and K. K.-W. Lo, *Organometallics*, 2012, **31**, 5844–5855; (g) E. E. Langdon-Jones, N. O. Symonds, S. E. Yates,

- A. J. Hayes, D. Lloyd, R. Williams, S. J. Coles, P. N. Horton and S. J. A. Pope, *Inorg. Chem.*, 2014, **53**, 3788–3797.
- 5 (a) V. Fernandez-Moreira, M. L. Ortego, C. F. Williams, M. P. Coogan, M. D. Villacampa and M. C. Gimeno, *Organometallics*, 2012, **31**, 5950–5957; (b) M. Bartholomä, J. Valliant, K. P. Maresca, J. Babich and J. Zubieta, *Chem. Commun.*, 2009, 493–512; (c) R. G. Balasingham, M. P. Coogan and F. L. Thorp-Greenwood, *Dalton Trans.*, 2011, **40**, 11663–11674; (d) V. Fernández-Moreira, F. L. Thorp-Greenwood, A. J. Amoroso, J. Cable, J. B. Court, V. Gray, A. J. Hayes, R. L. Jenkins, B. M. Kariuki, D. Lloyd, C. O. Millet, C. Williams and M. P. Coogan, *Org. Biomol. Chem.*, 2010, **8**, 3888–3901.
- 6 (a) M.-W. Louie, H.-W. Liu, M. H.-C. Lam, T.-C. Lau and K. K.-W. Lo, *Organometallics*, 2009, **28**, 4297–4307; (b) M.-W. Louie, H.-W. Liu, M. H.-C. Lam, Y.-W. Lam and K. K.-W. Lo, *Chem. – Eur. J.*, 2011, **17**, 8304–8308.
- 7 S. Clède, F. Lambert, R. Saint-Fort, M. A. Plamont, H. Bertrand, A. Vessières and C. Policar, *Chem. – Eur. J.*, 2014, **20**, 8714–8722.
- 8 (a) S. Hostachy, J.-M. Swiecicki, C. Sandt, N. Delsuc and C. Policar, *Dalton Trans.*, 2016, **45**, 2791–2279; (b) S. Clède and C. Policar, *Chem. – Eur. J.*, 2015, **21**, 942–958.
- 9 (a) A. E. Pierri, A. Pallaoro, G. Wu and P. C. Ford, *J. Am. Chem. Soc.*, 2012, **134**, 18197–18200; (b) I. Chakraborty, J. Jimenez, W. M. C. Sameera, M. Kato and P. K. Mascharak, *Inorg. Chem.*, 2017, **56**, 2863–2873; (c) S. J. Carrington, I. Chakraborty, J. M. L. Bernard and P. K. Mascharak, *Inorg. Chem.*, 2016, **55**, 7852–7858.
- 10 H. C. Kolb, M. G. Finn and K. B. Sharpless, *Angew. Chem., Int. Ed.*, 2001, **40**, 2004–2021.
- 11 (a) B. Schulze and U. S. Schubert, *Chem. Soc. Rev.*, 2014, **43**, 2522–2571; (b) J. D. Crowley and D. A. McMorran, *Top. Heterocycl. Chem.*, 2012, **28**, 31–83; (c) D. Schweinfurth, N. Deibel, F. Weisser and B. Sarkar, *Nachr. Chem.*, 2011, **59**, 937–941; (d) H. Struthers, T. L. Mindt and R. Schibli, *Dalton Trans.*, 2010, **39**, 675–696; (e) D. Schweinfurth, L. Hettmanczyk, L. Suntrup and B. Sarkar, *Z. Anorg. Allg. Chem.*, 2017, **643**, 554–584.
- 12 W. K. C. Lo, G. S. Huff, J. R. Cubanski, A. D. W. Kennedy, C. J. McAdam, D. A. McMorran, K. C. Gordon and J. D. Crowley, *Inorg. Chem.*, 2015, **54**, 1572–1587.
- 13 H. C. Bertrand, S. Clède, R. Guillot, F. Lambert and C. Policar, *Inorg. Chem.*, 2014, **53**, 6204–6223.
- 14 (a) B. Chen, Y. Li, W. Yang, W. Luo and H. Wu, *Org. Electron.*, 2011, **12**, 766–773; (b) K.-Y. Zhao, G.-G. Shan, Q. Fu and Z.-M. Su, *Organometallics*, 2016, **35**, 3996–4001.
- 15 C. Carayon and S. Fery-Forgues, *Photochem. Photobiol. Sci.*, 2017, **16**, 1020–1035 and references therein.
- 16 M. J. Stocks, D. R. Cheshire and R. Reynolds, *Org. Lett.*, 2004, **6**, 2969–2971.
- 17 L. Suntrup, S. Klenk, J. Klein, S. Sobottka and B. Sarkar, *Inorg. Chem.*, 2017, **56**, 5771–5783.
- 18 G. J. Stor, F. Hartl, J. W. M. van Outersterp and D. J. Stufkens, *Organometallics*, 1995, **14**, 1115–1131.
- 19 (a) N. M. Shavaleev, Z. R. Bell, T. L. Easun, R. Rutkaite, L. Swanson and M. D. Ward, *Dalton Trans.*, 2004, 3678–3688; (b) R. Czerwieńiec, A. Kapturkiewicz, J. Lipkowski and J. Nowacki, *Inorg. Chim. Acta*, 2005, **358**, 2701–2710; (c) X. Chen, F. J. Femia, J. W. Babich and J. Zubieta, *Inorg. Chim. Acta*, 2001, **314**, 91–96; (d) C. B. Anderson, A. B. S. Elliott, C. J. McAdam, K. C. Gordon and J. D. Crowley, *Organometallics*, 2013, **32**, 788–797; (e) S. V. Kumar, W. K. C. Lo, H. J. L. Brooks, L. R. Hanton and J. D. Crowley, *Aust. J. Chem.*, 2015, **69**, 489–498.
- 20 M. Obata, A. Kitamura, A. Mori, C. Kameyama, J. A. Czaplewska, R. Tanaka, I. Kinoshita, T. Kusumoto, H. Hashimoto, M. Harada, Y. Mikata, T. Funabikig and S. Yano, *Dalton Trans.*, 2008, 3292–3300.
- 21 T. Y. Kim, A. B. S. Elliott, K. J. Shaffer, C. J. McAdam, K. C. Gordon and J. D. Crowley, *Polyhedron*, 2013, **52**, 1391–1398.
- 22 (a) M. Wolff, L. Munoz, A. François, C. Carrayon, A. Seridi, N. Saffon, C. Picard, B. Machura and E. Benoist, *Dalton Trans.*, 2013, **42**, 7019–7031; (b) A. Boulay, A. Seridi, C. Zedde, S. Ladeira, C. Picard, L. Maron and E. Benoist, *Eur. J. Inorg. Chem.*, 2010, 5058–5062.
- 23 R. Eychenne, S. Guizani, J.-H. Wang, C. Picard, N. Malek, P.-L. Fabre, M. Wolff, B. Machura, N. Saffon, N. Lepareur and E. Benoist, *Eur. J. Inorg. Chem.*, 2017, **1**, 69–81.
- 24 Y. Zhao, R. Zhang, Y. Xu, H. Qi, X. Chen and C. Zhang, *J. Electroanal. Chem.*, 2015, **739**, 28–35.
- 25 P. Datta, D. Sarkar, A. P. Mukhopadhyay, E. Lopez-Torrez, C. J. Pastor and C. Sinha, *J. Organomet. Chem.*, 2011, **696**, 488–495.
- 26 (a) Y. Zhou, J. W. Kim, R. Nandhakumar, M. J. Kim, E. Cho, Y. S. Kim, Y. H. Jang, C. Lee, S. Han, K. M. Kim, J.-J. Kim and J. Yoon, *Chem. Commun.*, 2010, **46**, 6512–6514 and references therein; (b) G. V. Loukova, *Chem. Phys. Lett.*, 2002, **353**, 244–252.
- 27 (a) J. Jia, M. Cui, J. Dai and B. Liu, *Dalton Trans.*, 2015, **44**, 6406–6415; (b) L. Wei, J. W. Babich, W. Ouellette and J. Zubieta, *Inorg. Chem.*, 2006, **45**, 3057–3066; (c) M. V. Werrett, G. S. Huff, S. Muzzioli, V. Fiorini, S. Zacchini, B. W. Skelton, A. Maggiore, J. M. Malicka, M. Cocchi, K. C. Gordon, S. Stagni and M. Massi, *Dalton Trans.*, 2015, **44**, 8379–8393; (d) T. Klemens, A. Świtlicka-Olszewska, B. Machura, M. Grucela, H. Janeczek, E. Schab-Balcerzak, A. Szłapa, S. Kula, S. Krompiec, K. Smolarek, D. Kowalska, S. Mackowski, K. Erfurt and P. Lodowski, *RSC Adv.*, 2016, **6**, 56335–56352; (e) A. Świtlicka, T. Klemens, B. Machura, E. Schab-Balcerzak, K. Laba, M. Lapkowski, M. Grucela, J. Nycz, M. Szala and M. Kania, *RSC Adv.*, 2016, **6**, 112908–112918; (f) G.-W. Zhao, J.-H. Zhao, Y.-X. Hu, D.-Y. Zhang and X. Li, *Synth. Met.*, 2016, **212**, 131–141; (g) Y.-J. Pu, R. E. Harding, S. G. Stevenson, E. B. Namdas, C. Tedeschi, J. P. J. Markham, R. J. Rummings, P. L. Burn and I. D. W. Samuel, *J. Mater. Chem.*, 2007, **17**, 4255–4264.
- 28 C.-C. Hsu, C.-C. Lin, P.-T. Chou, C.-H. Lai, C.-W. Hsu, C.-H. Lin and Y. Chi, *J. Am. Chem. Soc.*, 2012, **134**, 7715–7724.

- 29 S. P. Anthony, *ChemPlusChem*, 2012, **77**, 518–531.
- 30 (a) V. Sathish, A. Ramdass, P. Thanasekaran, K.-L. Lu and S. Rajagopal, *J. Photochem. Photobiol., C*, 2015, **23**, 25–44; (b) L. Ravotto and P. Ceroni, *Coord. Chem. Rev.*, 2017, **346**, 62–76.
- 31 R. Katoh, K. Suzuki, A. Furube, M. Kotani and K. Tokumaru, *J. Phys. Chem. C*, 2009, **113**, 2961–2965.
- 32 (a) D. Schweinfurth, R. Pattacini, S. Strobel and B. Sarkar, *Dalton Trans.*, 2009, 9291–9297; (b) S. Hohloch, D. Schweinfurth, M. G. Sommer, F. Weisser, N. Deibel, F. Ehret and B. Sarkar, *Dalton Trans.*, 2014, **43**, 4437–4450; (c) D. Schweinfurth, S. Strobel and B. Sarkar, *Inorg. Chim. Acta*, 2011, **374**, 253–260.
- 33 G. Sheldrick, *Acta Crystallogr., Sect. A: Found. Adv.*, 2015, **71**, 3–8.
- 34 G. M. Sheldrick, *Acta Crystallogr., Sect. C: Struct. Chem.*, 2015, **71**, 3–8.
- 35 M. J. Frisch, G. W. Trucks, H. B. Schlegel, G. E. Scuseria, M. A. Robb, J. R. Cheeseman, G. Scalmani, V. Barone, B. Mennucci, G. A. Petersson, H. Nakatsuji, M. Caricato, X. Li, H. P. Hratchian, A. F. Izmaylov, J. Bloino, G. Zheng, J. L. Sonnenberg, M. Hada, M. Ehara, K. Toyota, R. Fukuda, J. Hasegawa, M. Ishida, T. Nakajima, Y. Honda, O. Kitao, H. Nakai, T. Vreven, J. A. Montgomery, J. E. Peralta, F. Ogliaro, M. Bearpark, J. J. Heyd, E. Brothers, K. N. Kudin, V. N. Staroverov, R. Kobayashi, J. Normand, K. Raghavachari, A. Rendell, J. C. Burant, S. S. Iyengar, J. Tomasi, M. Cossi, N. Rega, J. M. Millam, M. Klene, J. E. Knox, J. B. Cross, V. Bakken, C. Adamo, J. Jaramillo, R. Gomperts, R. E. Stratmann, O. Yazyev, A. J. Austin, R. Cammi, C. Pomelli, J. W. Ochterski, R. L. Martin, K. Morokuma, V. G. Zakrzewski, G. A. Voth, P. Salvador, J. J. Dannenberg, S. Dapprich, A. D. Daniels, O. Farkas, J. B. Foresman, J. V. Ortiz, J. Cioslowski and D. J. Fox, *Gaussian 09, Revision A.1*, Gaussian, Inc., Wallingford CT, 2009.
- 36 G. Zhurko and D. Zhurko, *ChemCraft 1.6*, 2011, <http://www.chemcraftprog.com/index.html>.
- 37 J. P. Perdew, K. Burke and M. Ernzerhof, *Phys. Rev. Lett.*, 1996, **77**, 3865–3868.
- 38 (a) P. J. Hay and W. R. Wadt, *J. Chem. Phys.*, 1985, **82**, 270–283; (b) P. J. Hay and W. R. Wadt, *J. Chem. Phys.*, 1985, **82**, 299–310.
- 39 W. J. Hehre, L. Radom, P. V. R. Schleyer and J. A. Pople, *Ab initio Molecular Orbital Theory*, Wiley, New York, 1986.
- 40 (a) B. Mennucci and J. Tomasi, *J. Chem. Phys.*, 1997, **106**, 5151–5158; (b) M. Cossi, V. Barone, B. Mennucci and J. Tomasi, *Chem. Phys. Lett.*, 1998, **286**, 253–260.
- 41 G. Velmurugan, B. K. Ramamoorthi and P. Venuganalingam, *Phys. Chem. Chem. Phys.*, 2014, **16**, 21157–21171.
- 42 K. Suzuki, A. Kobayashi, S. Kaneko, K. Takehira, T. Yoshihara, H. Ishida, Y. Shiina, S. Oishic and S. Tobita, *Phys. Chem. Chem. Phys.*, 2009, **11**, 9850–9860.
- 43 J. C. De Mello, H. F. Wittmann and R. H. Friend, *Adv. Mater.*, 1997, **9**, 230–232.